Dangling bond defects in SiC: An *ab initio* study

Blair R. Tuttle
Department of Physics, Penn State Behrend, Erie, Pennsylvania 16563 USA

(Received 6 September 2017; published 10 January 2018)

We report first-principles microscopic calculations of the properties of defects with dangling bonds in crystalline 3*C*-SiC. Specifically, we focus on hydrogenated Si and C vacancies, divacancies, and multivacancies. The latter is a generic model for an isolated dangling bond within a bulk SiC matrix. Hydrogen serves to passivate electrically active defects to allow the isolation of a single dangling-bond defect. We used hybrid density-functional methods to determine energetics and electrical activity. The present results are compared to previous 3*C*-SiC calculations and experiments. Finally, we identify homopolar carbon dangling-bond defects as the leakage causing defects in nanoporous SiC alloys.

DOI: 10.1103/PhysRevB.97.045203

I. INTRODUCTION

Silicon carbide (SiC) is a wide-band-gap, structurally stable semiconductor which is ideal for mechanical-electrical devices [1], for high-power electronics applications [2], and for use in high-temperature [3] and radiation-rich [4] environments. Point defects have been implicated in the degradation or limitation of material performance of SiC technology. Oxidized porous 3*C*-SiC was found to have isolated carbon dangling-bond (DB) defects [5]. Early studies of oxidized bulk 4*H*-SiC implicated silicon vacancies in limiting electronic device performance [6]. Radiation effects are important for space electronics and studies find a hydrogen-related shallow defect forms after high-energy hydrogen implantation [7]. Nanoporous SiC alloys are being implemented as back-end-of-the-line insulators for integrated circuits [8]. Experimental studies find deep defects are associated with leakage currents in nanoporous SiC capacitors [9–11]. The specific nature of the electrically active defects in SiC alloys depends on the growth conditions although DB defects are implicated in all cases [11].

Given the importance of point defects in various SiC-based technologies, there has been extensive research to identify the fundamental properties of point defects in various SiC materials. Experimentally, numerous studies have used electron paramagnetic resonance (EPR) to identify spin-active defects in SiC bulk samples [12,13] and device structures [6]. A combination of experimental methods is needed to correlate structural defects and electrical levels [14,15]. Theoretical calculations help identify specific defects from the variety of experimental signatures [12,13,16,17]. Most experimental studies focus on the 4*H*-SiC polytype since it is widely used in electronic devices. Fewer studies have examined defects in 3*C*-SiC [12,13]. EPR studies clearly identify vacancy defects in 3*C*-SiC. Electronic-structure calculations have confirmed experiments and provided information regarding the vacancy electrical levels [12,13,18]. Recent *ab initio* calculations identified intrinsic defects in 3*C*-SiC observed by photoluminescence [19]. Amorphous materials have gained interest due to the use of amorphous SiC alloys in silicon-based integrated-circuit technology. Early EPR experiments on amorphous SiC identified isolated carbon defects [20]. More recent studies have found similar defects in nanoporous SiC [11,21]. However, new theoretical calculations are needed to help identify the specific defect complexes that have been observed in nanoporous SiC.

In the present study, we examine single dangling-bond defects in hydrogen-passivated vacancy complexes. Since hydrogen is ubiquitous in electronic device processing, the present calculations are relevant for both crystalline and amorphous SiC-based devices. We examine carbon and silicon DB defects in vacancies, divacancies, and multivacancies. The latter models an isolated DB that may form at an interface or internal pore. Substitutional DB defects are studied to determine the influence of back-bonding atoms on the DB's electronic structure. Bonding disorder is important for understanding amorphous SiC alloys. Donor and acceptor levels are accurately determined for all DB defects considered. Carbon DBs with carbon back bonds ($C{\equiv}C_{DB}$) have donor levels near midgap and acceptor levels near the conduction band edge. Our results indicate the $C{\equiv}C_{DB}$ defect matches the experimental parameters for the leakage causing defects in nanoporous SiC dielectrics.

The rest of this paper is organized as follows. In Sec. II, the atomic models and electronic structure methods are described in detail. In Sec. III we report our main results. In Sec. IV we analyze our calculations. In Sec. V we discuss our results in the context of previous theoretical and experimental results. Finally, we conclude the paper in Sec. VI.

II. MODELS AND METHODS

To consider defects in 3*C*-SiC, we employ density-functional theory as implemented in the computer code VASP [22,23] (version 5.4.1) along with supercell structural models including 108 and 500 SiC units in the crystalline supercell structure. For Si and C, we treat the outer four valence electrons explicitly and use the projector augmented wave method to capture the effect of core electrons [24,25]. A plane-wave basis with an energy cutoff of 400 eV is used. For integrations over the Brillouin zone, it has long been understood that one can accelerate convergence by using special k points that avoid Brillouin zone edges [26]. Indeed, we find one special k point at

1/4 (111) is well converged for the size supercells considered. Spin polarization is employed when needed.

We treat exchange-correlation effects with the Perdew-Burke-Ernzerhof (PBE) functional [27]. We find that a theoretical equilibrium lattice constant of 4.38 Å matches the value found previously using the PBE [28] functional and is close to the experimental value. In order to correct for the errors due to the PBE functional, we employ a hybrid density-functional method [29] (HYB) including a mixture of the PBE [27] and nonlocal Fock exchange. In these calculations, we employ a mixing parameter of 0.17 but no screening parameter. The mixing parameter for the present HYB method results in a calculated band gap of 2.40 eV, which matches the experimental band gap. The room-temperature experimental band gap is 2.36 eV, whereas the low-temperature (~4 K) gap is 2.42 eV [30]. Previously, similar hybrid functionals for SiC accurately reproduced band gaps and other properties [18,28,31,32]. Computational resource restrictions prevent us from using HYB calculations for 500 SiC unit supercells. However, our HYB calculations for 108 SiC unit supercells are compared directly to the respective PBE results and a HYB correction term is established. It has recently been observed that for deep-level defects the PBE and HYB results are close if one employs a common reference [31,33]. For all defect-level calculations, we use the HYB 3*C*-SiC valence-band maximum as the common reference level.

For defect calculations, the supercell volume is held fixed while all atoms are relaxed until their forces are less than 0.01 eV/Å. We calculate defect charge transition energies ($\epsilon^{q/0}$) from the relaxed total energies using standard techniques [34,35]. We employ *ab initio* corrections for charged supercells [34,36]. Because large multivacancies are considered in this study, 500 SiC unit supercells are required to minimize finite supercell size effects. For the 500 SiC unit supercells, the energy corrections for charged supercells are less than 0.2 eV, as discussed in more detail below. For these large supercells, PBE calculations are employed using the HYB correction term.

As mentioned above, a hybrid correction term provides a correction to the PBE result in our 500 SiC supercell calculations. Specifically, the hybrid correction term (ΔE_{HYB}) is found by the energy difference in the raw PBE and HYB defect charge transition calculations: $\Delta E_{\mathrm{HYB}} = \epsilon^{q/0}_{\mathrm{HYB}} - \epsilon^{q/0}_{\mathrm{PBE}}$. The calculations include atomic relaxations but do not include charged defect corrections. The ΔE_{HYB} correction is calculated for smaller supercells based on 108 SiC units. The behavior of the correction terms is analyzed in detail below. All corrections are less than 0.5 eV and we estimate the uncertainty introduced is an order of magnitude smaller.

III. RESULTS

Here we report our results for the electronic properties of various DB defects in 3*C*-SiC. We report first our single pristine vacancy results and then we report results for hydrogenated vacancies.

A. Pristine vacancy results

Previous studies thoroughly describe the electronic structure of prestine vacancies in 3*C*-SiC [18,19]. In Fig. 1, we report the relative energies of a single vacancy in various charge states as a function of the Fermi level (E_{F}). Figure 1(a) shows the relative energetics for the bare carbon vacancy (V_{C}). In the neutral charge state, the energy of V_{C} is set to zero. Figure 1(b) shows the energetics for the bare silicon vacancy. The lowest energy configuration considered involves a neighboring carbon atom moving into the vacant silicon site. Formally, this structure can be considered a carbon vacancy/carbon substitutional complex ($V_{\mathrm{C}}\,C_{\mathrm{Si}}$). For both defect complexes considered in Fig. 1, some silicon DBs are interacting, which explains the similarities in the relative energetics of the various charge states. In both cases, the doubly positive charge state is the lowest energy state up to midgap. As the Fermi energy rises above midgap, charge transitions occur and for Fermi energies near the conduction band edge the negative charge state is favored. The present results are close to recent results using hybrid density-functional theory (DFT) [18] and DFT-GW [19] methods.

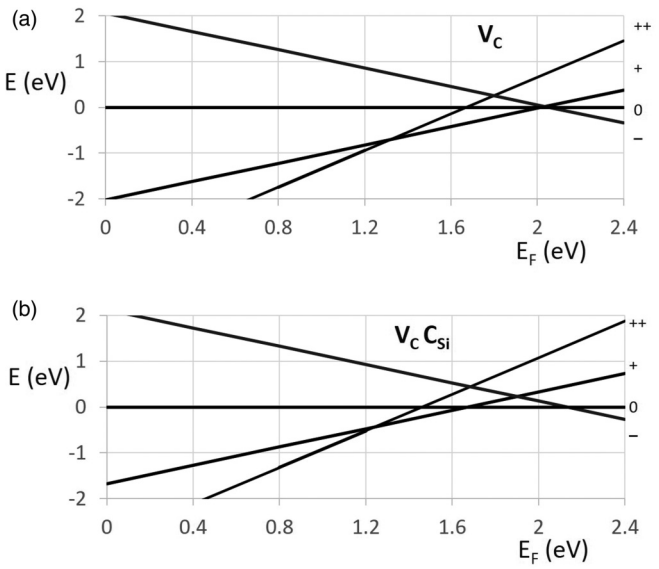

FIG. 1. Relative energy of vacancy defects in charge states (+2,+1,0,−1) versus Fermi energy (E_{F}).

B. Hydrogenated vacancy results

We report calculations for the defect properties of hydrogenated vacancy complexes. The main result is the thermodynamic transition levels, specifically the donor (+/0) and acceptor (0/−) levels for defects involving a single DB atom. We examine single hydrogenated vacancies (HV) with three passivating hydrogens and one DB. We examine the hydrogenated divacancy (HDV) where a Si and a neighboring C are removed from the supercell. The HDV complex includes five hydrogens passivating all but one of the DBs. For both the HV and HDV complexes, the DB defect's electron can interact with nearby hydrogen atoms. To examine a more isolated DB, we create a hydrogenated multivacancy (HMV) defect where we start with a single vacancy and then remove three of the four neighbors of the central defect atom. Nine hydrogens passivate DBs, leaving one isolated defect. This defect complex has been previously employed to examine isolated defects in bulk crystalline silicon [37].

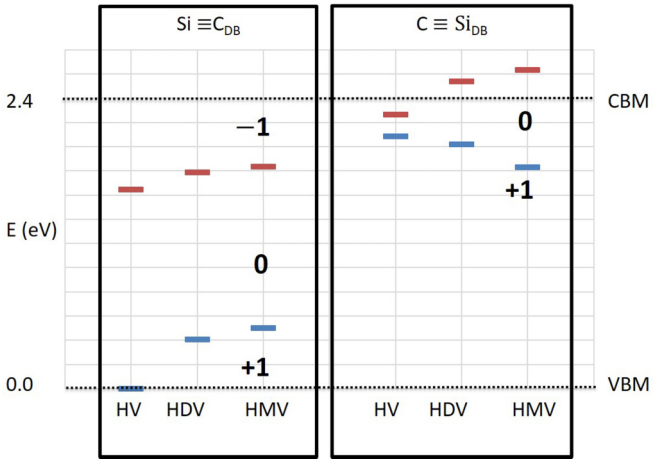

FIG. 2. Donor (blue) and acceptor (red) levels for heteropolar DBs in hydrogenated vacancy complexes.

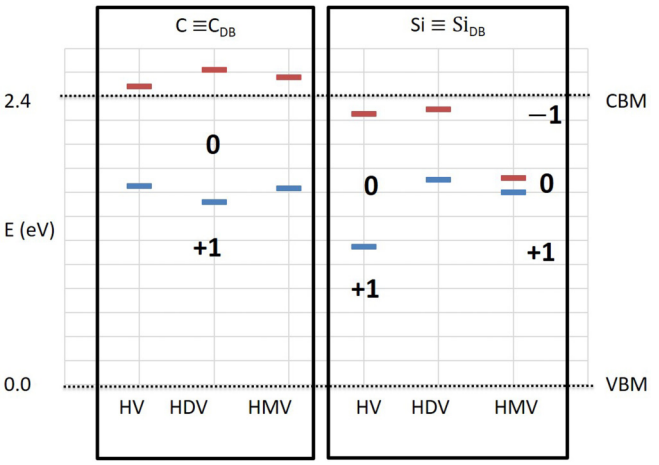

FIG. 3. Donor (blue) and acceptor (red) levels for homopolar DBs in hydrogenated vacancy complexes.

Because there is great interest in amorphous SiC environments where bonding disorder is common, we also consider the above hydrogenated vacancy defects with Si (C) substituting for the C (Si) DB atom. The result is a DB atom with the three back bonds of the same polarity, e.g., a silicon defect atom bonded to three silicons. The homopolar bonded defects differ from the standard defects where there are heteropolar back bonds, e.g., a silicon defect atom bonded to three carbons. Bonding polarity has significant effects on the DB's electronic structure.

The interaction of a defect's electron with back-bonding electrons is important. One measure of this interaction is the correlation energy: $U = \epsilon^{-/0} - \epsilon^{+/0}$, i.e., the difference between the acceptor and the donor level [38]. Small correlation energies indicate a defect with small electronic rearrangements upon charging and discharging. For instance, shallow substitutional defects have small ($U < 0.1$ eV) correlation energies, e.g., N_C in SiC. Large U values indicate significant electronic and structural rearrangements. Most of the present complexes result in large U values (i.e., $U > 0.5$ eV).

1. Heteropolar back bonding

In Fig. 2, in the left panel, we report the donor $(+/0)$ and acceptor $(0/-)$ levels for carbon DBs (Si≡C$_{DB}$) for the HV, HDV, and HMV complexes. For each complex, the donor level is in the bottom half of the gap and the acceptor level is in the top half. The Si≡C$_{DB}$ defects show small variations between the three environments considered. The donor and acceptor levels shift up slightly between the single-vacancy and multivacancy environments. The correlation energies are similar for each environment: 1.6, 1.4, and 1.3 eV for the Si≡C$_{DB}$ HV, HDV, and HMV defects, respectively. The similarity in the three results suggests little interaction between the defect state and the surrounding hydrogens in the HV and HDV cases.

In Fig. 2, in the right panel, we report the donor $(+/0)$ and acceptor $(0/-)$ levels for silicon DBs (C≡Si$_{DB}$) for the HV, HDV, and HMV complexes. For each complex, the donor level is the top half of the band gap and the acceptor level is near the conduction band edge. The C≡Si$_{DB}$ defects vary between the three environments considered. The donor (acceptor) levels shift down (up) slightly between the single vacancy and multivacancy environments. The correlation energies vary from 0.2 eV for the single vacancy to 0.5 eV for the multivacancy environment.

For the hydrogenated carbon vacancy, the present study found that in the positive charge state two distinct local minima structures have the same energy, with the energy difference being less than 0.01 eV. In one structure, there is one Si DB and three Si–H bonds, whereas in the other structure there are two Si–H bonds and one three-center (Si–H–Si) bond. In an earlier study, singly hydrogenated carbon vacancies were found to exhibit a similar three-center hydrogen bond [39]. Three center hydrogen bonds are commonly found in semiconductor vacancies [40].

2. Homopolar back bonding

In Fig. 3, in the left panel, we report the donor $(+/0)$ and acceptor $(0/-)$ levels for carbon DBs (C≡C$_{DB}$) for the HV, HDV, and HMV complexes. For each complex, the donor level is just above midgap and the acceptor level is just above the conduction band minimum. The C≡C$_{DB}$ defects show very small variations between the three environments considered. The donor and acceptor levels vary by less than 0.2 eV between the three environments. The C≡C$_{DB}$ defect involves a central carbon with C–C bond lengths of 1.57 Å in all three environments. Small physical relaxations occur as the charge state of the defect changes. For instance, the C–C bond length is the same within ±0.01 Å for each charge state. The large correlation energy, $\sim +0.9$ eV, indicates there is significant electronic rearrangement.

In Fig. 3, in the right panel, we report the donor $(+/0)$ and acceptor $(0/-)$ levels for silicon DBs (Si≡Si$_{DB}$) for the HV, HDV, and HMV complexes. The Si≡Si$_{DB}$ defect levels show no clear trend between the three environments considered. Physically, the Si DB moves out from its initial 3C-SiC crystalline position. The final Si–Si back-bond lengths are ∼2.28 Å with little variation (<0.02 Å) between environments. The correlation energies are 1.1, 0.2, and 0.1 eV for the HV, HDV, and HMV complexes, respectively.

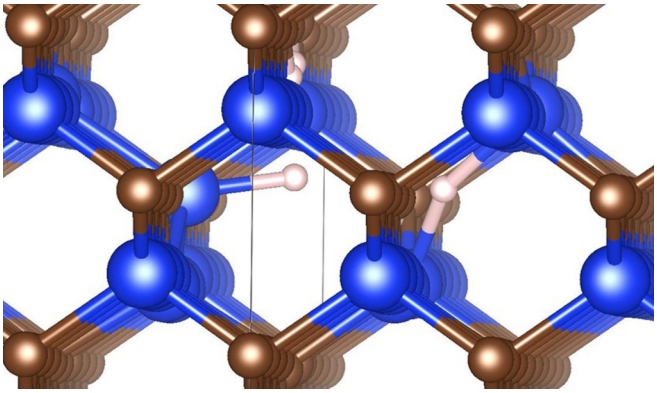

FIG. 4. Ball-and-stick model of hydrogenated divacancy complex with a three-center Si–H–Si bond in the positive charge state. Balls of white, gray (blue), and dark (brown) are for hydrogen, silicon, and carbon, respectively. The gray vertical line represents the supercell edge.

In the $Si{\equiv}Si_{DB}$ HDV complex, a three-center Si–H–Si bond forms in the positive charge state. Figure 4 shows a ball-and-stick model of the final positions for the hydrogenated divacancy $Si{\equiv}Si_{DB}$ complex in the positive charge state. The blue, brown, and white balls represent silicon, carbon, and hydrogen, respectively. As pictured in Fig. 4, the silicon with homopolar back bonds is passivated with a hydrogen. In the positive charge state, hydrogen strongly prefers forming a Si≡Si–H bond over a C≡Si–H bond. The system favors a symmetric three-center bond, C≡Si–H–Si≡C over one with mixed back bonding.

IV. ANALYSIS

A. Carbon DB electron density

Because the carbon DB transition levels are relatively independent of the surrounding environment, examining the DB defect spin density of the multivacancy HMV complex provides insight for all environments. Specifically, the differences between the $Si{\equiv}C_{DB}$ and the $C{\equiv}C_{DB}$ transition levels reported in Figs. 2 and 3 can be explained in terms of defect spin-density differences.

Figure 5 shows the ball-and-stick figures for the neutral charge state of the carbon DB defect. The yellow (gray) shaded region around the carbon DBs is an isosurface of the electron spin density for the gap-level eigenstate. In Fig. 5(a) the electron isosurface for $Si{\equiv}C_{DB}$ indicates the defect state is mainly a carbon nonbinding p-orbital electron, whereas in Fig. 5(b) the $C{\equiv}C_{DB}$ has significant electron density additionally spread to the C–Si secondary back bonds.

The differences in the charge densities for the two defects indicate variations in occupation of molecular bonding energy levels. For the $C{\equiv}C_{DB}$ neutral defect, charge is transferred from the C–Si bonding sp^3 state to the higher energy defect state. Therefore, the $C{\equiv}C_{DB}$ neutral defect state is relatively higher in energy than the $Si{\equiv}C_{DB}$ defect state. Removing the defect electron from the $C{\equiv}C_{DB}$ neutral defect state is favored. This is the qualitative explanation for why the donor $(+/0)$ level of the $C{\equiv}C_{DB}$ complex is higher in the gap than the donor level of the $Si{\equiv}C_{DB}$ defect.

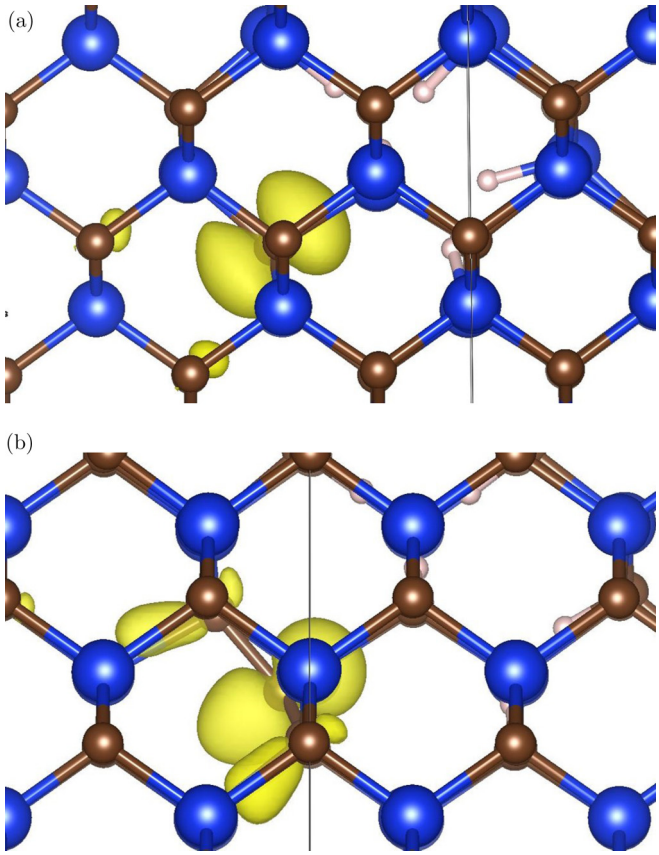

FIG. 5. Ball-and-stick model of hydrogenated multivacancy complex with a carbon DB defect with (a) silicon back bonds and (b) carbon back bonds. Balls of white, gray (blue), and dark (brown) are for hydrogen, silicon, and carbon, respectively. The gray vertical line represents the supercell edge.

B. Charged supercell corrections

Because of the finite size of supercells, defect calculations suffer from spurious interactions between a defect and its periodic image, as discussed in detail elsewhere [34]. The main corrections to be considered here are those due to the charged supercells. We employ *ab initio* corrections for charged supercells [34,36] using the experimental dielectric constant of 9.7 for screening. The correction to the total energy is 0.096 eV for singly charged defects in 500 SiC unit supercells. In addition, there is a potential alignment correction term. Corrections for charged supercells have predictable effects on the thermodynamic transition levels. Specifically, the corrections generally lower the donor $(+/0)$ level and raise the acceptor $(0/-)$ level.

Figure 6 reports the charged supercell energy corrections for the 12 charged defects considered in this study. The dashed line represents the 0.096-eV constant shift whereas the dots indicate the total correction. For most defects considered, the potential alignment correction is less than 0.05 eV, although for the HMV defects the correction is ∼0.1 eV. For donor and acceptor levels, the average charged supercell correction is −0.05 and +0.11 eV, respectively. Therefore, the charged supercell correction terms have a modest effect on the transition gap levels.

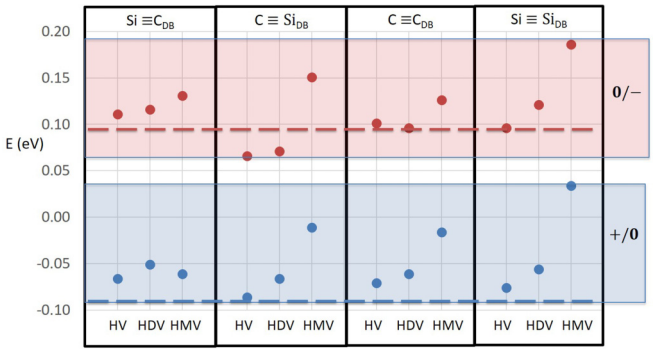

FIG. 6. Charged supercell corrections for donor (bottom) and acceptor (top) levels. Dashed line represents the constant correction and the dots are the total corrections for each model as discussed in text.

C. HYB corrections

The PBE exchange-correlation functional is semilocal and is insufficient in calculations where nonlocal effects are important. Defect levels within PBE have long suffered from the band-gap error. For instance, our PBE band gap for 3C-SiC is 1.37 eV, which is similar to previous PBE results [41] but about 1 eV lower than experiment. The relative band edges for our PBE and HYB calculations are aligned using the average local potential. Comparing our PBE and HYB bulk results, we find the PBE band-gap error is split between a valence-band error of $\Delta\mathrm{VBM} = 0.62\,\mathrm{eV}$ and a conduction-band error of $\Delta\mathrm{CBM} = 0.41\,\mathrm{eV}$. Previous studies found that deep transition levels in PBE and hybrid PBE are very similar if one uses a common reference [31,33].

Figure 7 reports the HYB correction term (ΔE_{HYB}) for each structural defect considered in the present study. Half of the corrections are within ± 0.1 eV, indicating PBE is reasonable for these structures. The acceptor levels for the Si≡C$_{\mathrm{DB}}$ defects show the lowest corrections ($<0.03\,\mathrm{eV}$). Other DBs show no clear trends regarding the HV, HDV, and HMV environments. To further analyze the corrections, in Fig. 8 we report the HYB correction term (ΔE_{HYB}) versus Fermi level for the defect levels from the hydrogenated defects considered. There is a trend that donor levels are corrected to lower energies and acceptor levels are corrected to higher ones. This trend is consistent with defect states being partially hybridized with

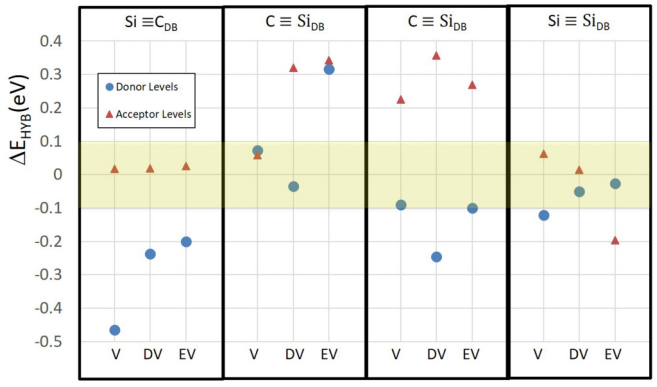

FIG. 7. HYB correction energy (ΔE_{HYB}) for transition levels considered.

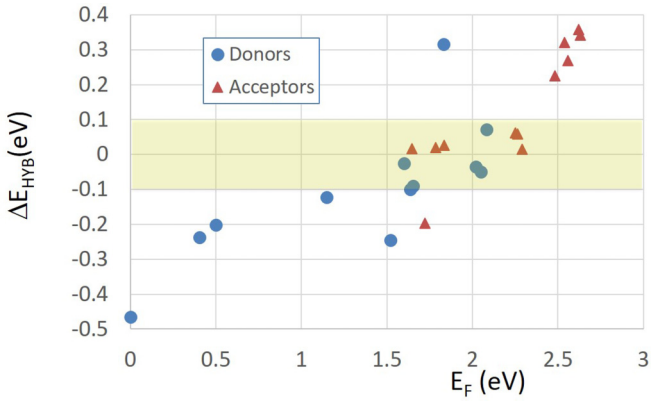

FIG. 8. HYB correction energy (ΔE_{HYB}) for transition levels versus Fermi level (E_{F}).

the nearest bands. From Fig. 8, one can see that the five defects with $\Delta E_{\mathrm{HYB}} > +0.2\,\mathrm{eV}$ are for acceptor levels above the conduction band edge. These can be considered "shallow" defects even though they are not experimentally accessible. Similarly, the donor levels below Fermi level of 0.5 eV have $\Delta E_{\mathrm{HYB}} < -0.2\,\mathrm{eV}$. Naturally, these shallow levels shift significantly since the hybrid calculations shift the band edges by several tenths of an eV. Overall, our calculations confirm previous studies indicating that deep defects are generally well represented by PBE [31,33].

V. DISCUSSION

Next, we discuss the present calculations in the context of previous work. The present calculations are directly relevant to studies of defects in 3C-SiC. Similar defects occur in amorphous SiC alloys. The theoretical calculations here in crystalline 3C-SiC can be used as a starting point for understanding defects in amorphous alloys, similar to the use of crystalline Si calculations to understand defects in amorphous silicon [42].

A. Defects in crystalline SiC

The present results for pristine vacancy defects (with no hydrogen passivation) are close to those reported in Ref. [18]. However, the present transition levels are a few tenths of an eV lower in the gap. One possible source of the difference may be the differing charge supercell corrections. In the present study, we use supercells with a lattice constant of 21.9 Å and fully *ab initio* correction methods [36]. In Ref. [18], smaller supercells are used (lattice ∼13 Å) and a semiempirical correction formula is employed for charge supercell corrections. An ∼0.2-eV difference in charge correction would explain the discrepancies between the present work and Ref. [18]. However, other parameter differences may be involved. For integration over the Brillouin zone, the present study employs a single special k point, whereas Ref. [18] employs a $2\times2\times2$ Γ-centered grid. In Ref. [18], a screened hybrid functional is employed, whereas in the present study there is no screening. Instead, we adjust the mixing parameter to match the theoretical and experimental band gaps. A full examination of all these factors is beyond the scope of the present study.

Silicon carbide devices are used in radiation-rich environments where puzzling new defects can emerge. An experimental study on 200-keV hydrogen implanted 4*H*-SiC concludes that one shallow defect emerged near (∼0.2 eV) the valence band edge, which was deduced to be hydrogen related [7]. Numerous defect complexes occur during irradiation. In fact, the experiments of Ref. [7] found several defects unrelated to hydrogen. Common single-vacancy defect levels are all far from the valence band edge as illustrated in the present calculations reported in Fig. 1. However, a silicon vacancy or divacancy partially passivated with hydrogens (see Fig. 2) results in defect levels near the valence band edge, which may explain the defect observed in the hydrogen implant study.

Experimental studies on oxidized porous microcrystalline 3*C*-SiC revealed an EPR active carbon defect analogous to the well-known P_b defect at the Si/SiO_2 interface [5]. Samples were first annealed in a hydrogen-forming gas to passivate EPR active defects. Subsequently, the samples were vacuum annealed to reveal some of the original EPR signal. One EPR defect was identified as carbon related and the hydrogen activation energy was 4.3 ± 0.3 eV.

We use PBE to calculate the hydrogen binding energy in the multivacancy defects. Hydrogen prefers passivating carbon with (heteropolar back bonds) silicon back bonds ($Si{\equiv}C_{DB}$) by 0.5 eV or more. The bonding of hydrogen to $Si{\equiv}Si_{DB}$ is the least favored of the four defects considered. The passivation energy of ($Si{\equiv}Si_{DB}$) is 1.2 eV less than ($Si{\equiv}C_{DB}$). To compare to the vacuum annealing experiments, we calculate the energy of a H atom in vacuum using an empty supercell with sides ∼13 Å. The present calculations treat the hydrogen as a classical particle so a 0.2-eV zero-point energy is used to account for the quantum nature of the hydrogen when bonded [42]. Also, we add the 0.2-eV barrier energy for the diffusion of hydrogen though a silicon oxide [43]. The total barrier energy for the release of hydrogen from a heteropolar back-bonded carbon DB ($Si{\equiv}C_{DB}{-}H$) is calculated to be 4.3 eV, matching the experimental value of 4.3 ± 0.3 eV. This binding energy is also close to the value previously calculated for heteropolar back-bonded C–H bonds on 2*H*-SiC surfaces [44]. The present calculations confirm the assignment of the experimentally observed EPR active defect in Ref. [5] as a heteropolar back-bonded carbon DB.

B. Defects in amorphous SiC alloys

Nanoporous SiC alloys are a new class of amorphous materials that are grown from molecular precursors. These materials have low dielectric constants, are structurally stable, and have been used as insulators within integrated silicon technologies [45]. In a 2013 study, experiments used electrically detected magnetic resonance to identify defects responsible for spin-dependent tunneling in nanoporous SiC [9]. Samples with low oxygen content are relevant to current theoretical calculations. Low-oxygen samples, with concentrations less than 1%, have band gaps between 2.4 and 2.7 eV, close to the 2.4-eV band gap of 3*C*-SiC. In the experiments, neutral defects are spin-recombination centers as electrons tunnel through the nanoporous SiC sample. Based on the line shape and g value observed, the study concludes that a carbon DB is responsible for leakage. From electrical measurements, the neutral defect level was placed in the top half of the band gap. More recent studies on nanoporous SiOC alloys [11] confirm the earlier experiments on SiC alloys [9], indicating that isolated carbon DBs are the primary leakage-causing defects. Early tight-binding calculations put carbon sp^3 and sp^2 DB levels at the bottom half of the SiC band gap [46]. Our state-of-the-art calculations provide an explanation for the above discrepancy between theory and experiment.

The present *ab initio* results show that both $Si{\equiv}C_{DB}$ and $C{\equiv}C_{DB}$ are mainly *p-orbital* carbon DBs (see Fig. 5). However, the back-bonding dramatically influences the position of the electrical level. The heteropolar back-bonded carbon DB (with silicon back bonds) has a neutral level in the bottom half of the SiC band gap (see Fig. 2) consistent with early tight-binding results. However, the homopolar back-bonded carbon DB (with back-bonded carbons) has a neutral defect level in the top half of the SiC band gap for reasons discussed in Sec. IV above. In summary, we find the homopolar back-bonded carbon DB ($C{\equiv}C_{DB}$) defect is consistent with the interpretation from experiments of leakage in nanoporous SiC [9].

Reference [9] also examined the influence of thermal treatments on the bonding of nanoporous SiC alloys. As the temperature was raised from 400 to 700 °C, the Si–H concentration decreased, whereas the C–H concentration remained the same. This observation is consistent with the present calculations showing the Si–H is much weaker than the C–H bond strength. Interestingly, as hydrogen is released from Si–H bonds homopolar bonding is reduced [9]. There may be postdeposition treatments that allow hydrogens from Si–H bonds to passivate carbon DBs.

VI. CONCLUSIONS

We report first-principles calculations for dangling bond defects in 3*C*-SiC. Calculations involve large supercells to minimize finite-size errors. A hybrid exchange-correlation functional (HYB) is employed to accurately treat defects over the experimental band gap. Motivated by interest in isolated DBs that are present in SiC-based devices, we focus our study on hydrogenated vacancy models to examine single DBs. The donor and acceptor levels for DBs are reported in Figs. 2 and 3. We vary the size of the vacancy complex and the nature of the back-bonded atoms. The physical and electronic structure are examined in specific cases (Figs. 4 and 5). We discuss the application of the current results to understand previous theory and experiment. For deep-level defects, PBE and HYB results agree with each other, to within 0.1 eV, consistent with previous theory [33]. We corroborate the experimental assignment of silicon-back-bonded carbon DBs found in porous oxidized 3*C*-SiC. We conclude that carbon-back-bonded carbon DBs match the leakage-causing defects observed in nanoporous SiC-based capacitors [9].

ACKNOWLEDGMENTS

This research was funded by NSF Grant No. RUI-DMR 1506403. This research was conducted using Advanced Cyber Infrastructure computational resources provided by The Institute for Cyber Science at The Pennsylvania State University (http://ics.psu.edu).

[1] C. A. Zorman and R. J. Parro, in *Silicon Carbide* (Wiley-VCH, Weinheim, 2009), pp.411–451.

[2] G. Liu, B. R. Tuttle, and S. Dhar, Appl. Phys. Rev. **2**, 021307 (2015).

[3] J. B. Casady and R. W. Johnson, Solid-State Electron. **39**, 1409 (1996).

[4] P. J. Sellin and J. Vaitkus, Nucl. Instrum. Methods Phys. Res., Sect. A **557**, 479 (2006).

[5] J. L. Cantin, H. J. V. Bardeleben, Y. Ke, R. P. Devaty, and W. J. Choyke, Appl. Phys. Lett. **88**, 092108 (2006).

[6] C. J. Cochrane, P. M. Lenahan, and A. J. Lelis, Appl. Phys. Lett. **100**, 023509 (2012).

[7] G. Alfieri and T. Kimoto, New J. Phys. **10**, 073017 (2008).

[8] A. Grill, S. M. Gates, T. E. Ryan, S. V. Nguyen, and D. Priyadarshini, Appl. Phys. Rev. **1**, 011306 (2014).

[9] T. A. Pomorski, B. C. Bittel, C. J. Cochrane, P. M. Lenahan, J. Bielefeld, and S. W. King, J. Appl. Phys. **114**, 074501 (2013).

[10] T. A. Pomorski, B. C. Bittel, P. M. Lenahan, E. Mays, C. Ege, J. Bielefeld, D. Michalak, and S. W. King, J. Appl. Phys. **115**, 234508 (2014).

[11] M. J. Mutch, P. M. Lenahan, and S. W. King, J. Appl. Phys. **119**, 094102 (2016).

[12] J. Isoya, T. Umeda, N. Mizuochi, N. T. Son, E. Janzén, and T. Ohshima, Phys. Stat. Solidi B **245**, 1298 (2008).

[13] M. Bockstedte, A. Gali, A. Mattausch, O. Pankratov, and J. W. Steeds, Phys. Stat. Solidi B **245**, 1281 (2008).

[14] K. Kawahara, X. T. Trinh, N. T. Son, E. Janzén, J. Suda, and T. Kimoto, Appl. Phys. Lett. **102**, 112106 (2013).

[15] T. Aichinger, P. M. Lenahan, B. R. Tuttle, and D. Peters, Appl. Phys. Lett. **100**, 112113 (2012).

[16] X. Shen and S. T. Pantelides, Mat. Sci. Forum **717–720**, 445 (2012).

[17] B. R. Tuttle, T. Aichinger, P. M. Lenahan, and S. T. Pantelides, J. Appl. Phys. **114**, 113712 (2013).

[18] T. Oda, Y. Zhang, and W. J. Weber, J. Chem. Phys. **139**, 124707 (2013).

[19] F. Bruneval and G. Roma, Phys. Rev. B **83**, 144116 (2011).

[20] T. Christidis, M. Tabbal, S. Isber, M. A. El Khakani, and M. Chaker, Appl. Surf. Sci. **184**, 268 (2001).

[21] V. V. Afanas'ev, K. Keunen, A. Stesmans, M. Jivanescu, Z. Tőkei, M. R. Baklanov, and G. P. Beyer, Microelectron. Eng. **88**, 1503 (2011).

[22] G. Kresse and J. Hafner, Phys. Rev. B **47**, 558 (1993).

[23] G. Kresse and J. Furthmüller, Phys. Rev. B **54**, 11169 (1996).

[24] P. E. Blöchl, Phys. Rev. B **50**, 17953 (1994).

[25] G. Kresse and D. Joubert, Phys. Rev. B **59**, 1758 (1999).

[26] D. J. Chadi and M. L. Cohen, Phys. Rev. B **8**, 5747 (1973).

[27] J. P. Perdew, K. Burke, and M. Ernzerhof, Phys. Rev. Lett. **77**, 3865 (1996).

[28] T. Oda, Y. Zhang, and W. J. Weber, Chem. Phys. Lett. **579**, 58 (2013).

[29] P. Broqvist, A. Alkauskas, and A. Pasquarello, Phys. Rev. B **80**, 085114 (2009).

[30] *Group IV Elements, IV-IV and III-V Compounds. Part b - Electronic, Transport, Optical and Other Properties*, edited by O. Madelung, U. Rössler, and M. Schulz (Springer, Berlin, 2002), pp. 1–25.

[31] A. Alkauskas, P. Broqvist, and A. Pasquarello, Phys. Rev. Lett. **101**, 046405 (2008).

[32] F. Devynck, A. Alkauskas, P. Broqvist, and A. Pasquarello, Phys. Rev. B **84**, 235320 (2011).

[33] C. Freysoldt, B. Lange, J. Neugebauer, Q. Yan, J. L. Lyons, A. Janotti, and C. G. Van de Walle, Phys. Rev. B **93**, 165206 (2016).

[34] C. Freysoldt, B. Grabowski, T. Hickel, J. Neugebauer, G. Kresse, A. Janotti, and C. G. Van de Walle, Rev. Mod. Phys. **86**, 253 (2014).

[35] S. Lany and A. Zunger, Phys. Rev. B **78**, 235104 (2008).

[36] C. Freysoldt, J. Neugebauer, and C. G. Van de Walle, Phys. Rev. Lett. **102**, 016402 (2009).

[37] B. Tuttle, C. G. Van de Walle, and J. B. Adams, Phys. Rev. B **59**, 5493 (1999).

[38] C. Herring, N. M. Johnson, and C. G. Van de Walle, Phys. Rev. B **64**, 125209 (2001).

[39] B. Aradi, A. Gali, P. Deák, J. E. Lowther, N. T. Son, E. Janzén, and W. J. Choyke, Phys. Rev. B **63**, 245202 (2001).

[40] B. Szûcs, A. Gali, Z. Hajnal, P. Deák, and C. G. Van de Walle, Phys. Rev. B **68**, 085202 (2003).

[41] J. Wiktor, G. Jomard, M. Torrent, and M. Bertolus, Phys. Rev. B **87**, 235207 (2013).

[42] C. G. Van de Walle and R. A. Street, Phys. Rev. B **49**, 14766 (1994).

[43] B. Tuttle, Phys. Rev. B **61**, 4417 (2000).

[44] B. R. Tuttle and S. T. Pantelides, Surf. Sci. **656**, 109 (2017).

[45] W. Volksen, R. D. Miller, and G. Dubois, Chem. Rev. **110**, 56 (2009).

[46] J. Robertson, Philos. Mag. B **66**, 615 (1992).